Graph measures in task-based fMRI: Functional integration during read-out of visual and auditory information

Laura Quante[1,2☯], **Daniel S. Kluger**[1,2☯]*, **Paul C. Bürkner**[1], **Matthias Ekman**[3], **Ricarda I. Schubotz**[1,2,4]

1 Department of Psychology, University of Münster, Münster, Germany, **2** Otto-Creutzfeldt-Center for Cognitive and Behavioral Neuroscience, University of Münster, Münster, Germany, **3** Donders Institute for Brain, Cognition and Behaviour, Radboud University Nijmegen, Nijmegen, Netherlands, **4** Department of Neurology, University Hospital Cologne, Cologne, Germany

☯ These authors contributed equally to this work.
* d.kluger@wwu.de

Abstract

This study investigated how attending to auditory and visual information systematically changes graph theoretical measures of integration and functional connectivity between three network modules: auditory, visual, and a joint task core. Functional MRI BOLD activity was recorded while healthy volunteers attended to colour and/or pitch information presented within an audiovisual stimulus sequence. Network nodes and modules were based on peak voxels of BOLD contrasts, including colour and pitch sensitive brain regions as well as the dorsal attention network. Network edges represented correlations between nodes' activity and were computed separately for each condition. Connection strength was increased between the task and the visual module when participants attended to colour, and between the task and the auditory module when they attended to pitch. Moreover, several nodal graph measures showed consistent changes to attentional modulation in form of stronger integration of sensory regions in response to attention. Together, these findings corroborate dynamical adjustments of both modality-specific and modality-independent functional brain networks in response to task demands and their representation in graph theoretical measures.

Introduction

Integration and segregation in global brain communication are necessary prerequisites for complex behavior [1–3]. While segregation means that distributed areas work independently from one another and serve specialised functions, integration denotes a global coordinative coupling of functionally distinct brain regions.

Using network analysis and graph theoretical measures, the human brain has been shown to be organised in functionally specialised modules [4–8] and a small number of highly connected and topologically central brain regions, the *connective core* (also called *rich club*; [9–

12]). The core's connectivity profile makes it the ideal structure to integrate information from different brain regions. Following Shanahan's *connective core hypothesis* [13], this central module enables and guides communication between all other brain regions. Parallel computation and competition between brain regions–as coordinated by the connective core—result in the formation of dynamic coalitions of specific brain regions, which in turn determine behavior. Such coalitions are formed in a serial manner, corresponding to a sequential shift between states of integration and segregation [3, 13–14].

Empirical studies have indeed shown that the level of integration within the brain changes depending on task demands [15–18]. Cohen and D'Esposito, for example, found that a working memory task was accompanied by greater integrative communication within the brain when compared to a simple motor task [18]. In addition, Cole and colleagues [19] demonstrated that the fronto-parietal network shows flexible functional connectivity depending on task demands, supporting the idea of a connective core dynamically orchestrating brain processes. Further support for this idea was provided by Ekman and colleagues [20]: In their study, participants prepared for a colour/motion discrimination task. During preparation, colour regions showed higher integration with core regions when colour discrimination was prepared, and reduced integration when motion discrimination was prepared (vice versa for motion regions). In other words, connections between core and periphery dynamically and systematically changed depending on the task to prepare.

In the present study, we investigated changes in core-periphery interaction when participants attended to auditory vs. visual information. Participants were required to attend to colour, pitch, or both colour and pitch information in an audiovisual stimulus sequence. To ensure modality-specific attentional engagement, subjects were asked to not only attend to but read out visual and auditory information to perform a visual search task at the end of each sequence. Importantly, when they interpreted colour, pitch or both colour and pitch as requested, this visual search was facilitated, and performance was enhanced. Note that we defined the joint task network as "core" whereas visual and auditory areas were defined as "periphery". Functionally, the joint task network was specific to the present paradigm and taken to reflect the translation of pitch and/or colour information into the spatial domain for the subsequent search task. Based on Shanahan [13] and in line with Ekman and colleagues [20], we hypothesised temporarily stronger links between task core and task-relevant sensory areas. Specifically, we expected increased functional connectivity between the core and the visual module when participants attended to visual stimuli, and between core and the auditory module when participants attended to auditory stimuli. In either case, there should be stronger integration of the task-specific regions within the network. We assessed integration in terms of functional connectivity and different graph theoretical measures.

Materials and methods

Participants

Twenty-eight right-handed volunteers (18–29 years, mean 23.7 ± 2.83 SD years old, 7 male) with normal or corrected-to-normal vision participated in the experiment after giving written informed consent. None of them reported a history of medical, neurological or psychiatric disorders or substance abuse. Participants were compensated with course credit or payment. Two additional participants were excluded because of drop out and heavy leg movements during the fMRI session. The study protocol was conducted in accordance with ethical standards of the Declaration of Helsinki and approved by the local ethics committee of the University of Münster.

Task

Participants exploited auditory and visual information from a 12-second stimulus sequence to subsequently predict the location of a target in a visual search display (Fig 1). Every trial started with a fixation cross (200 ms) followed by a cue (1300 ms). The deterministic cue indicated which source of information was predictive of the target location and therefore allowed participants to focus on auditory information (A) and/or visual information (V). The cues consisted of two letters (*VA*, *VX*, *AX*, or *XX*) and instructed participants to read out both visual and auditory information (VA), only auditory information (AX), only visual information (VX), or that neither modality was informative (XX). If indicated by the cue, visual information (colour) predicted that the target would appear in the upper or lower half of the search display (e.g., red–upper half, blue–lower half) and auditory information (pitch) indicated that the target would appear in the right or left half of the search display (e.g., high–right half, low–left half). Stimulus-target associations (i.e., red/blue colour–upper/lower half and low/high pitch–right/left side) were balanced across participants. Importantly, in case of condition VA, participants could restrict their visual search to one quarter of the search display, in condition VX and AX to one half. In condition XX, visual search could not be spatially restricted.

The end of the audiovisual sequence was followed by a fixation cross (200 ms) and a blank screen (500 ms) before the visual search display appeared. When the search display appeared, participants were asked to respond with their right index finger to indicate when they detected the target. Next, the response display showed up and participants indicated whether the target was a regular letter "L" (left middle finger) or rotated (left index finger). After the second button press, the next trial started.

Every participant was presented 48 VA trials, 24 VX trials, 24 AX trials, and 48 XX trials in pseudo-randomised order, with overall balanced transition probabilities.

Stimuli

Audio-visual sequences. Participants were presented sequences of 11 audio-visual stimuli which consisted of a visual pattern and a piano-like chord played simultaneously. The visual

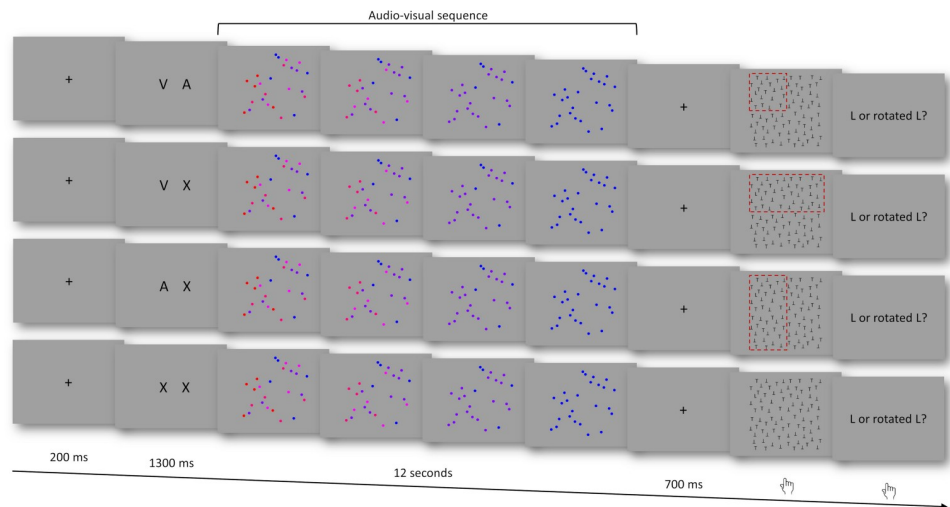**Fig 1. Illustration of the trial design for the four experimental conditions.** The area framed in red represents the display location that could be predicted by the participant based on information provided by the audio-visual sequence (note that during the real presentation, no red frame was visible). Functional connectivity analysis was based on data recorded during the entire audio-visual sequence (12 s).

pattern was a random arrangement of 25 non-overlapping coloured dots, with a dot diameter of 0.3˚ of visual angle. The dot cloud covered a square area of about 7˚ of visual angle and was centered on the screen. Each dot was coloured in one of the following five colours: red (RGB values: 255, 0, 0), blue (0, 0, 255), or intermediate mixtures thereof (255, 0, 128; 255, 0, 255; 128, 0, 255). The background was grey (160, 160, 160). Individual stimuli were created with *MATLAB* (The MathWorks, Inc., Natick, Massachusetts, USA) and compiled to videos with *Windows Movie Maker* (Microsoft Cooperation). In each video, stimuli 1 to 10 were presented for 1250 ms, and the last stimulus was presented for 2000 ms. There was a crossfading period of 250 ms, where participants were presented a merged image of two consecutive stimuli. This created a smooth transition from one stimulus to another, resulting in a video duration of 12 seconds. Each video started with a standard stimulus, consisting of a balanced mixture of coloured dots (5 dots per colour). Over the course of the next 10 stimuli presented in each trial, dots changed their colour incrementally until every dot had the same colour (either red or blue). We generated eight different standard stimuli and three types of stepwise changes, leading to 2 final states (red, blue) x 8 standard stimuli x 3 sequence types = 48 different videos.

Auditory stimuli were constructed using synthetic string samples from the *EastWest Colossus sound library* (Native Instruments, Berlin, Germany). Trials were made up of ten successive variations of a five-note *standard* chord (C^{maj9}, c–d–e–g–b): Starting with the chord split over five octaves (one note per octave, lasting 1000 ms), notes were individually transposed to the next octave in pseudorandom order every 1000 ms. Following a transposition, the respective note resonated for another 250 ms, creating a smooth transition between chord variations. This way, all notes were gradually shifted upwards or downwards over the course of an auditory sequence until the final chord (lasting 2000 ms) exclusively comprised notes from either the highest or the lowest octave. All notes and corresponding frequencies across octaves are shown in Table 1. As for the visual sequences, we generated 48 different auditory sequences.

For every participant, auditory and visual sequences were randomly paired to build 12 audio-visual sequences of each type (as classified by the final stimulus: blue-high, blue-low, red-high and red-low). Every audio-visual sequence was presented three times per participant: once within condition VA, once within condition XX and once within conditions VX or AX.

Visual search display. The visual search display consisted of 80 black letters "T" (Calibri font, 0.4 x 0.2˚ of visual angle), 40 of which were presented upright and the other 40 upside-down, on a grey background (160, 160, 160). Letters were randomly distributed in a square area of 8.7˚ of visual angle. For each trial, one letter "T" was replaced by the target (L or rotated L).

Procedure

The experiment was programmed and run using *Presentation* software (Neurobehavioral Systems, San Francisco, CA, USA).

Participants completed a training session on the first day. The training session comprised 12 trials to learn the association between colour (red and blue) and display location (upper and

Table 1. Notes and corresponding frequencies in Hz across octaves.

		Octave				
		2	3	4	5	6
Note	c	65.41	130.81	261.63	523.25	1046.50
	d	73.42	146.83	293.66	587.33	1174.66
	e	82.41	164.81	329.63	659.25	1318.51
	g	98.00	196.00	392.00	783.99	1567.98
	b	123.47	246.94	493.88	987.77	1975.53

lower half, respectively), 12 trials to learn the association between pitch (high and low) and display location (right and left half, respectively), as well as 24 trials to learn the association between the combination of colour and pitch and the corresponding display quarter. Afterwards, participants performed 48 training trials of the actual paradigm, i.e. using colour and pitch information to prepare for the upcoming target location (condition VA).

On the second day, the experiment was carried out in the fMRI scanner. Before the experiment, an echo planar imaging sequence was turned on and participants manually adjusted the sound volume. The scanner session was followed by a questionnaire evaluating the participants' behavior during the session (e.g., strategies, concentration, and difficulties performing the task).

Data acquisition

Whole-brain images were collected on a 3T Siemens Magnetom Prisma MR tomograph (Siemens, Erlangen, Germany) using a 20-channel head coil. Functional images were acquired using a gradient $T2^*$-weighted single-shot gradient-echo planar sequence sensitive to BOLD contrast (64×64 data acquisition matrix, 192 mm field of view, 90˚ flip angle, repetition time = 2000 ms, echo time = 30 ms). Each volume consisted of 33 adjacent axial slices with a slice thickness of 3 mm and a gap of 1 mm, resulting in a voxel size of $3 \times 3 \times 4$ mm^3. Images were acquired in interleaved order parallel to the AC-PC line to provide a whole-brain coverage. Structural data were acquired for each participant using a standard Siemens 3-D T1-weighted MPRAGE sequence for detailed reconstruction of anatomy with isotropic voxels ($1 \times 1 \times 1$ mm^3) in a 256-mm field of view (256×256 matrix, 192 slices, repetition time = 2130 ms, echo time = 2.28 ms). Participants' hands were placed on four-button response boxes. Index and middle fingers were placed on the response buttons. To minimise head motion, the head was tightly fixated with cushions, and earplugs were provided to attenuate scanner noise. Auditory stimuli were presented via headphones (MR confon, Magdeburg, Germany). Visual stimuli were projected on a screen positioned behind the participant's head by a video projector (JVC, Bad Vilbel, Germany). Participants viewed the screen by a 45˚ mirror, which was fixated on the top of the head coil and adjusted for each participant to provide a good view of the entire screen.

Behavioral data analysis

Behavioral performance was assessed via error rates and reaction times of correctly answered trials. To test for differences between conditions, pairwise t-tests were conducted using the statistic software package R (R Foundation for Statistical Computing, Vienna, Austria). Results of the paired t-tests were corrected for multiple comparisons at $p < .05$ using Bonferroni correction.

fMRI data analysis

fMRI data preprocessing. Brain image preprocessing and basic statistical analyses were conducted using *SPM12* (Wellcome Trust Centre for Neuroimaging, London, United Kingdom). Functional images were realigned based on three rotation and three translation parameters, slice time corrected, and co-registered to the structural scan. Structural scans were segmented into grey matter, white matter and cerebrospinal fluid. Structural and functional scans were normalised to the Montreal Neuroimaging Institute (MNI) template. Functional images were high-pass filtered (128 s period cutoff) and spatially smoothed with an 8 mm FWHM Gaussian kernel. For connectivity analyses, we additionally performed linear detrending and despiking, and regressed out the six realignment parameters, their temporal

derivatives, and the first five PCA components for both white matter and ventricle voxels from the unsmoothed preprocessed functional images using the *CONN* toolbox [21]. For confound removal, the toolbox uses the aCompCor strategy [22].

Design specifications. Event-related BOLD responses were estimated using a general linear model approach. The model comprised a total of 15 regressors plus intercept. Regressors of interest represented the four main conditions (VA, VX, AX, and XX), each modeled with an event duration of 12 seconds and convolved with the canonical hemodynamic response function. As regressors of nuisance, we included right and left button presses, cue presentation, visual search and area restriction of the search (as a parametric effect with levels -1, 0, and 1 corresponding to full display, half of the display, and quarter of the display, respectively), as well as the six realignment parameters. The first four regressors of nuisance were convolved with the canonical hemodynamic response function, with the first three being defined as actual events and with visual search being modeled with an event duration corresponding to the reaction time of that trial. Four contrasts were generated for each participant: VX>AX, VA>XX, VX>XX, and AX>XX. For each voxel, resulting contrast weights entered one-sample t-tests. General task activations (i.e., attention to visual stimuli, auditory stimuli, or both) were assessed by the conjunction VA>XX ∩ VX>XX ∩ AX>XX. To correct for multiple comparisons, false discovery rate (FDR) correction was used ($p < .05$).

Network construction. Nodes represented contrast peak voxels, and edges were defined as correlations between confound-corrected BOLD time series (*BOLD series* hereafter). Sixteen peak voxels were chosen from contrast VA>XX ∩ VX>XX ∩ AX>XX, and six peak voxels each from contrasts VX>AX and AX>VX, resulting in a total of 28 nodes. Every node was created by surrounding the corresponding peak voxel with a 6-mm-radius sphere using *AFNI*'s *3dUndump* and used to average, for every participant, BOLD series of voxels within a sphere ($n_{voxels} = 33$; see [23]). This approach aims to get reliable time series averages while simultaneously retaining a certain degree of functional node specificity.

Averaged BOLD series were used to calculate Pearson correlations between all pairs of nodes. Correlation coefficients were Fisher's Z transformed. To generate condition-specific correlation matrices, BOLD series were restricted to relevant volumes from the audio-visual sequences (six TRs per trial) of correctly answered trials, shifted by six seconds to account for the hemodynamic lag. In case of conditions VA and XX, 24 correctly answered trials were randomly chosen to balance the number of trials between conditions (minimum number of trials per subject and condition was 22). Accordingly, every correlation coefficient was based on at least 132 data points.

Matrix construction was done by using customised Python code (Python Software Foundation), utilizing the packages *NumPy* and *NiBabel*, and resulted in one 28 x 28 matrix per participant and condition (112 matrices in total). Connection strength was represented by positive and negative correlation coefficients, whereas negative correlations were set to zero for graph measure calculation (average percentage of negative correlations = 26.6%, range = 6.9–49.7%). MATLAB and the *Brain Connectivity Toolbox* [24] were used to compute connection strength and weighted graph measures. Nodes were grouped into three modules based on contrasts (task module: VA>XX ∩ VX>XX ∩ AX>XX, visual module: VX>AX, and auditory module: AX>VX). The joint task network represented the core of all brain areas involved in task performance.

Network analysis. To measure integration and core-periphery interaction, we analyzed connection strengths within and between modules and nodal graph measures by fitting generalised linear multilevel models (GLMMs, [25]). These models include fixed and random effects and thereby account for intra-individual homogeneity and inter-individual heterogeneity [26]. The R package *brms* [27–28], an interface to the programming language *Stan* ([29]; http://mc-stan.org/), was used to estimate the GLMMs in a Bayesian framework [30–31]. We used the

default priors of brms, which are chosen to be only weakly informative, thus having only negligible impact on the obtained estimates [27]. The posterior distribution over model parameters was estimated by means of a Markov Chain Monte Carlo procedure and the NUTS sampling algorithm [32] was used to draw samples (two independent chains with 2000 iterations each, of which the first 1000 were used as warm-up, leaving a total of 2000 posterior samples). The mean of the posterior distribution and a credible interval (usually a two-sided 95% credible interval; 95% CI) were used to summarise each model parameter. A 95% CI can be interpreted in the way that a given parameter lies within this interval with 95% probability. If desired, a parameter can be interpreted as significantly different from zero (on a 5% level) if the corresponding 95% CI does not contain zero. In all models, effect coding was used, which means that group means are contrasted with the grand mean by setting a reference category of every independent variable to -1. Because it cannot be assumed that graph measures are normally distributed [33], we chose response distributions that best fit the observed data. Convergence of all Bayesian GLMMs was assessed via the effective sample size for each parameter and the Gelman-Rubin statistic Rhat [34].

To quantify effects of connection type (i.e. within-module and between-modules connections), and attentional modulation on connection strength, we analyzed the data by fitting a GLMM with fixed effects of *visual read-out* (VR; yes, no), *auditory read-out* (AR; yes, no) and *connection type* (CT; visual-visual, auditory-auditory, core-core, visual-auditory, visual-core, auditory-core) and random effects for participant and node. The model specification in R formula (brms) was: Connection Strength ~ VR * AR * CT + (VR * AR | participant) + (VR * AR | node). We chose a skewed normal distribution to describe the distribution of the dependent variable, because the distribution of correlations was right-skewed. For effect coding, the following categories were chosen as reference (i.e., coded with -1): connection type = core-core, visual read-out = no, and auditory read-out = no.

In addition to connection strength, we calculated the following seven weighted graph measures for every node to quantify topological features of the network: betweenness centrality, characteristic path length, clustering coefficient, core closeness, nodal efficiency, participation coefficient, and strength (see S1 Table for detailed information).

For each graph measure, we fitted a GLMM with fixed effects of *visual read-out* (VR; yes, no), *auditory read-out* (AR; yes, no) and *module* (MOD; visual, auditory, core) and random effects for participant and node. The model specification in R formula (brms) was: Graph Measure ~ VR * AR * MOD + (VR * AR | participant) + (VR * AR | node). For effect coding, the following categories were chosen as reference (i.e., coded with -1): module = core, visual read-out = no, and auditory read-out = no.

Results

Behavioral results

Performance during training and fMRI session was assessed through error rates and reaction times on correctly answered trails. The average error rate of the fourth part of the training, which corresponded to condition VA, was 3.27% ($\pm$ 3.42 SD) and the average reaction time was 1659.80 ms ($\pm$ 527.91 SD), both demonstrating participants' ability to perform the task correctly. The average error rate of the fMRI session was 1.61% ($\pm$ 1.52 SD; range 0–4.86%) and did not differ significantly between conditions ($p > .05$ for all pairwise t-tests). The average reaction time was 2507.48 ms ($\pm$ 613.93 SD) and differed significantly between conditions ($p \leq .001$ for all pairwise t-tests), indicating that participants used the provided visual and auditory information to predict the target location. See Fig 2 and Table 2 for average reaction times and error rates per condition.
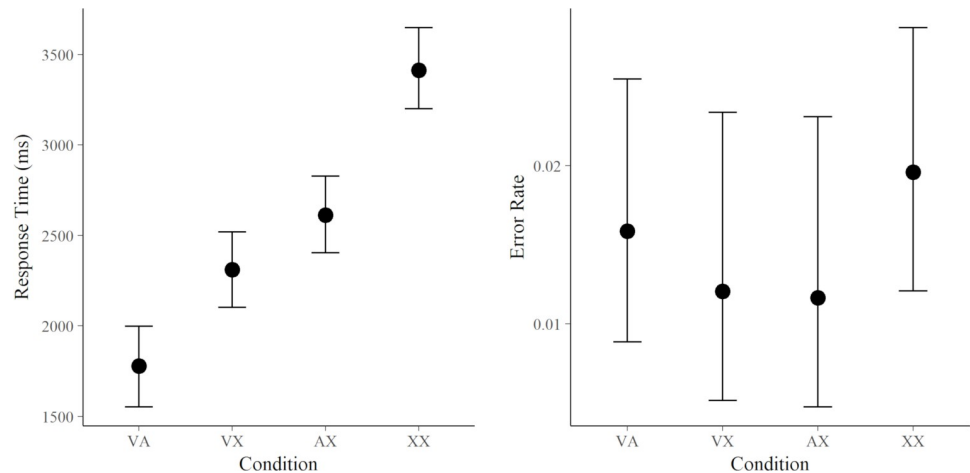
Fig 2. Mean reaction times and error rates for each condition of the fMRI experiment. Error bars represent confidence limits (95%). VA = visual and auditory read-out, VX = only visual read-out, AX = only auditory read-out, XX = control condition (no read-out). Reaction times show that visual search was not informed (restricted) in the XX condition, more restricted in the VX and the AX conditions, and most restricted in the VA condition.

fMRI results

Contrasts. In order to derive nodes for our network analysis, we focused on the following three contrasts (see Table 3): Group-level activations related to visual read-out (VX > AX) were found bilaterally in the occipital cortex and fusiform gyrus (BA 18/19/37) and in the superior parietal lobule (BA 7). We used the three most strongly activated voxels of the biggest cluster within the left and right hemisphere as nodes. The reverse contrast (AX > VX), representing auditory read-out, revealed significant bilateral activations in the superior temporal gyrus (BA 22). As nodes we used the three peak voxels of the left cluster, the peak voxel of the right cluster and two additional right hemisphere voxels, which corresponded to the significant left hemisphere voxels. This procedure ensured equal numbers of nodes within the visual and auditory modules. The conjunction of visual and/or auditory read-out relative to the passive condition (VA>XX ∩ VX>XX ∩ AX>XX) yielded significant bilateral activations in the superior and inferior parietal lobule along the intraparietal sulcus (BA 7/39/40), in the dorsal premotor cortex and inferior frontal junction (BA 6/44), and in lobule VI of the cerebellum. Sixteen voxels were chosen from this contrast to represent nodes of the task module.

Network analysis. Mean, standard deviation and range of all conditions are provided for graph measures and connection strength in S2 Table. All GLMMs converged successfully with an effective sample size of 300 or more for every relevant parameter and Rhat values of less than 1.1.

Connection strength of all connection types differed from the grand mean, with within-module connections being stronger and between-module connections being weaker (see Fig 3 and Table 4). When visual information was read out, connections between the visual and task

Table 2. Mean and standard deviation of reaction times and error rates during the fMRI session. Condition abbreviation see text and legend of Fig 2.

	VA	VX	AX	XX
Reaction time (ms)	1551 (549)	2211 (735)	2657 (917)	3611 (749)
Error rate (%)	1.64 (2.49)	1.19 (2.23)	1.19 (2.50)	2.01 (2.57)

Table 3. Peak voxel and local maxima.

Area		MNI coordinates x	y	z	z-value	p-value	Cluster size	p-value	Node
Visual (VX > AX)									
Occipital cortex and fusiform gyrus (BA 18/19/37)	L	-27	-88	2	5.79	< .001	1287	< .001 (< .001)	yes
		-42	-70	-10	5.44	< .001			yes
		-33	-76	-13	5.37	< .001			yes
Occipital cortex and fusiform gyrus (BA 18/19/37), superior parietal lobule (BA 7)	R	33	-82	5	5.78	< .001	1892	< .001 (< .001)	yes
		42	-73	-7	5.49	< .001			yes
		48	-61	-10	5.45	< .001			yes
		24	-55	56	4.74				no
Superior parietal lobule (BA 7)	L	-18	-58	68	4.12	.001	221	.004 (.044)	no
		-27	-55	62	3.97	.002			no
Thalamus	L	-18	-31	11	3.75	.003	114	.028 (.279)	no
Prefrontal cortex (BA 10/32)	L	-12	38	-4	3.61	.005	258	.002 (.024)	no
Putamen	R	36	-7	2	3.59	.005	153	.013 (.140)	no
Auditory (AX > VX)									
Superior temporal gyrus (STG; BA 22/41/42)	L	-54	-37	17	4.64	.022	60	.008 (.011)	yes
		-65	-34	11	3.48		n.s.		yes
		-66	-25	5	2.47		n.s.		yes
	R	66	-34	11	4.62	.022	125	< .001 (.001)	yes
		54	-34	11	4.28	.022			yes
		66	-25	5	4.27	.022			yes
Task (VA>XX ∩ VX>XX ∩ AX>XX)									
Inferior and superior parietal lobule (BA 7/39/40)	L	-33	-43	41	5.98	< .001	993	< .001 (< .001)	yes
		-27	-55	44	5.98	< .001			yes
		-18	-70	53	5.09	< .001			yes
Inferior and superior parietal lobule (BA 7/39/40)	R	12	-64	56	4.59	< .001	323	< .001 (.002)	yes
		30	-55	41	4.50	< .001			yes
Dorsal premotor cortex and inferior frontal junction (BA 6/44)	L	-45	2	26	5.26	< .001	1011	< .001 (< .001)	yes
		-57	5	20	5.16	< .001			yes
		-30	-1	59	4.87	< .001			yes
		-5	6	57	3.76				yes
	R	42	5	26	4.94	< .001	431	< .001 (< .001)	yes
		24	2	59	4.22	.001			yes
		36	-4	41	4.07	.002			yes
Cerebellum (lobule VI)	L	-24	-64	-25	4.04	.002	113	.015 (.148)	yes
		-27	-55	-28	3.98	.002			yes
		-12	-70	-25	3.46	.009			yes
	R	30	-64	-25	4.10				yes

Note. Shown are local peaks of significant clusters (n.s. = not significant).

module were stronger ($b = 0.007$, 95%-CI = [0.003, 0.011]) and connections within the auditory module were weaker ($b = -0.009$, [-0.017, -0.001]; see Fig 4). When auditory information was read out, connections between the auditory and task module ($b = 0.008$, [0.004, 0.011])
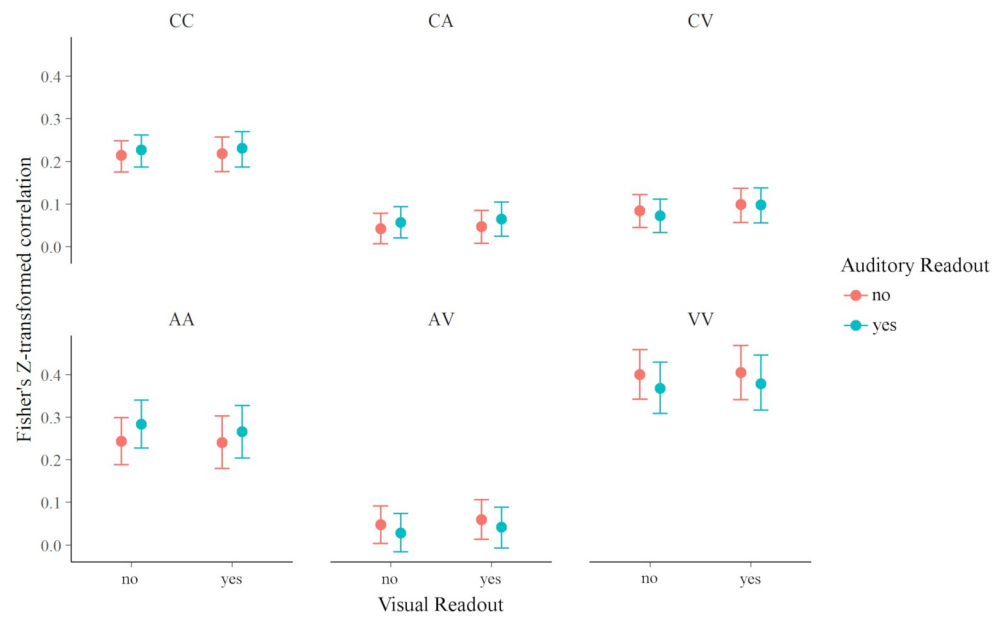
Fig 3. Connection strength for each connection type. Error bars represent 95% credible intervals. CC = connections within the task core, CA = connections between task core and auditory module, CV = connections between task core and visual module, AA = connections within auditory module, AV connections between auditory and visual module, VV = connections within visual module.

Table 4. GLMM for connection strength: Fixed effects.

Population-Level Effect	Estimate	l-95% CI	u-95% CI	
Intercept	0.176	0.141	0.210	*
VR_yes	0.003	-0.003	0.009	
AR_yes	0.001	-0.005	0.007	
CT_TA	-0.122	-0.143	-0.103	*
CT_TV	-0.087	-0.108	-0.067	*
CT_AA	0.082	0.042	0.124	*
CT_AV	-0.131	-0.148	-0.113	*
CT_VV	0.212	0.172	0.254	*
VR_yes * AR_yes	0.000	-0.004	0.005	
VR_yes * CT_TA	0.000	-0.004	0.004	
VR_yes * CT_TV	0.007	0.003	0.011	*
VR_yes * CT_AA	-0.009	-0.017	-0.001	*
VR_yes * CT_AV	0.003	-0.002	0.008	
VR_yes * CT_VV	0.000	-0.007	0.008	
AR_yes * CT_TA	0.008	0.004	0.011	*
AR_yes * CT_TV	-0.004	-0.007	0.000	
AR_yes * CT_AA	0.015	0.008	0.023	*
AR_yes * CT_AV	-0.010	-0.015	-0.005	*
AR_yes * CT_VV	-0.015	-0.023	-0.007	*
VR_yes * AR_yes * CT_TA	0.001	-0.003	0.004	
VR_yes * AR_yes * CT_TV	0.002	-0.001	0.006	
VR_yes * AR_yes * CT_AA	-0.004	-0.011	0.003	
VR_yes * AR_yes * CT_AV	0.000	-0.004	0.005	
VR_yes * AR_yes * CT_VV	0.001	-0.006	0.008	

Note. Credible intervals not including zero are marked with *. VR = visual read-out, AR = auditory read-out,

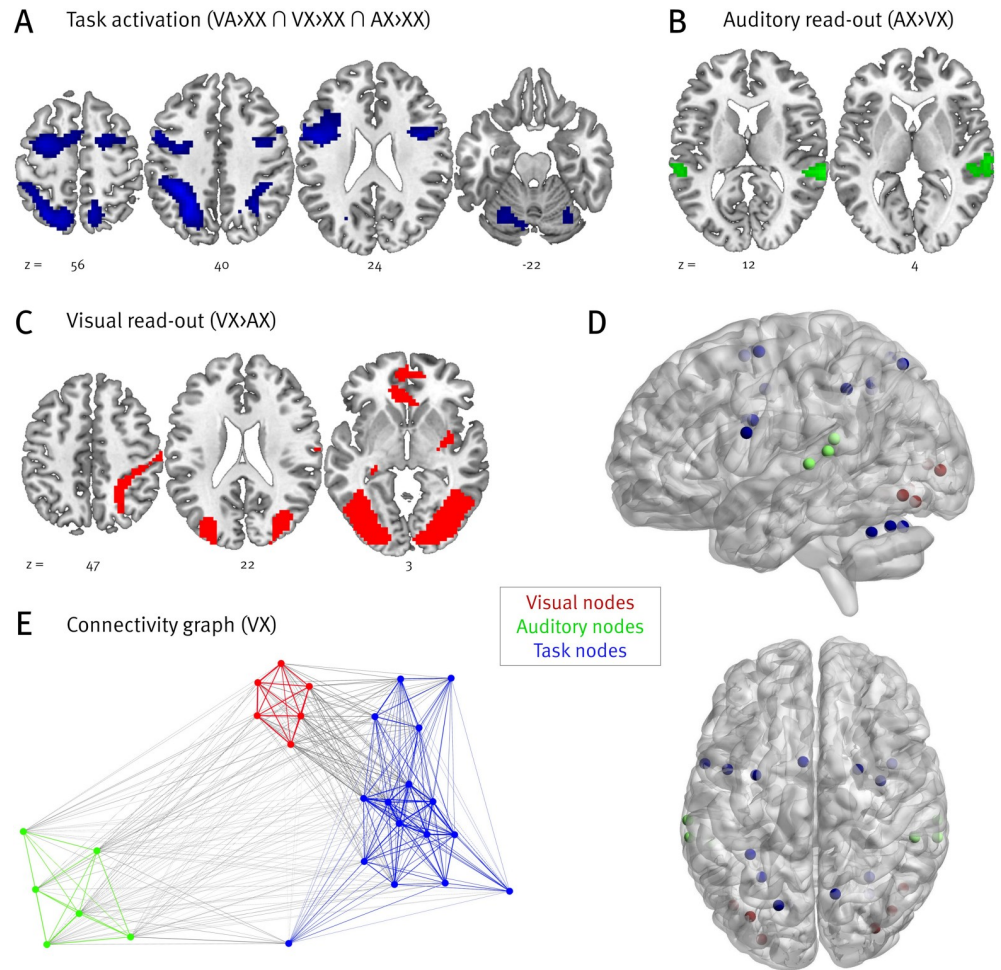CT = connection type with A = auditory, T = task, V = visual.

Fig 4. (A)–(C) Significant activations of the three contrasts of interest (FDR corrected, $p < .05$). (D) Nodes of the network analysis based on contrasts. The figure was generated with BrainNet Viewer [35]. (E) Connectivity graph of condition VX; only positive connections are displayed. A similar module structure was observed for conditions VA, AX, and XX. The figure was generated with Gephi [36] using the ForceAtlas2 algorithm [37]. Arrangement of nodes and edge width are based on connectivity strength.

and connections within the auditory module were stronger ($b = 0.015$, [0.008, 0.023]), and connections within the visual module ($b = -0.015$, [-0.023, -0.007]) and connections between the visual and auditory module were weaker ($b = -0.01$, [-0.015, -0.005]).

Table 5 displays credible intervals for the population-level effects of the GLMMs fitted for each graph measure.

Nodes within the auditory module had longer paths to other nodes ($b = 0.118$, 95%-CI [0.061, 0.174]), showed reduced clustering ($b = -0.208$, [-0.298, -0.116]), a greater distance to the core (i.e., task module; $b = -0.236$, [-0.326, -0.146]), decreased efficiency ($b = -0.019$, [-0.028, -0.010]) and decreased strength ($b = -0.262$, [-0.404, -0.117]) as well as higher participation in different modules ($b = 0.063$, [0.021, 0.105]), when compared to the grand mean.

Nodes within the visual module showed higher participation in different modules ($b = 0.042$, [0.001, 0.081]), when compared to the grand mean.

When auditory information was read out, auditory nodes had shorter paths to other nodes ($b = -0.019$, [-0.028, -0.010], showed enhanced clustering ($b = 0.037$, [0.018, 0.055]), a smaller

Table 5. Credible intervals of fixed effects of graph measure GLMMs.

Population-Level Effect	Betweenness centrality	Characteristic path length	Clustering coefficient	Core closeness	Nodal efficiency	Participation coefficient	Strength
Intercept	**[2.88; 3.32]**	**[1.73; 1.88]**	**[-1.94; -1.71]**	**[-4.63; -4.43]**	**[0.157; 0.181]**	**[0.439; 0.505]**	**[1.16; 1.42]**
VR_yes	[-0.10; 0.03]	[-0.04; 0.00]	[-0.01; 0.04]	[-0.00; 0.03]	[0.000; 0.006]	[-0.001; 0.014]	[-0.00; 0.04]
AR_yes	[-0.08; 0.04]	[-0.03; 0.01]	[-0.02; 0.04]	[-0.00; 0.04]	[-0.002; 0.005]	[-0.009; 0.001]	[-0.01; 0.04]
MOD_aud	[-0.35; 0.30]	**[0.06; 0.17]**	**[-0.30; -0.12]**	**[-0.33; -0.15]**	**[-0.028; -0.010]**	**[0.021; 0.105]**	**[-0.40; -0.12]**
MOD_vis	[-0.31; 0.32]	[-0.09; 0.02]	[-0.02; 0.18]	[-0.15; 0.03]	[-0.006; 0.014]	**[0.001; 0.081]**	[-0.05; 0.24]
VR_yes * AR_yes	[-0.09; 0.04]	[-0.02; 0.01]	[-0.03; 0.02]	[-0.02; 0.02]	[-0.002; 0.003]	[-0.005; 0.006]	[-0.02; 0.02]
VR_yes * MOD_aud	[-0.14; 0.04]	[-0.00; 0.02]	[-0.03; 0.01]	[-0.02; 0.01]	[-0.004; 0.000]	[-0.006; 0.006]	[-0.04; 0.01]
VR_yes * MOD_vis	[-0.07; 0.11]	**[-0.02; -0.002]**	[-0.00; 0.04]	**[0.01; 0.03]**	[0.000; 0.003]	[-0.007; 0.006]	[-0.00; 0.04]
AR_yes * MOD_aud	[-0.05; 0.13]	**[-0.03; -0.01]**	**[0.02; 0.06]**	**[0.01; 0.04]**	**[0.001; 0.004]**	[-0.004; 0.007]	**[0.02; 0.07]**
AR_yes * MOD_vis	[-0.15; 0.04]	**[0.02; 0.04]**	**[-0.06; -0.03]**	**[-0.04; -0.02]**	**[-0.005; -0.002]**	[-0.008; 0.003]	**[-0.08; -0.03]**
VR_yes * AR_yes * MOD_aud	[-0.13; 0.05]	[-0.00; 0.02]	[-0.02; 0.02]	[-0.02; 0.01]	[-0.002; 0.001]	[-0.008; 0.004]	[-0.03; 0.01]
VR_yes * AR_yes * MOD_vis	[-0.08; 0.10]	[-0.02; 0.00]	[-0.01; 0.02]	[0.00; 0.03]	[-0.001; 0.002]	[-0.004; 0.008]	[-0.01; 0.04]

Note. Credible intervals not including zero are written in bold. VR = visual read-out, AR = auditory read-out, MOD = module with vis = visual, aud = auditory.

distance to the core (b = 0.024, [0.012, 0.036]), and increased efficiency (b = 0.002, [0.001, 0.004] as well as increased strength (b = 0.046, [0.023, 0.069]). The opposite pattern was observed for visual nodes: They had longer paths to other nodes (b = 0.026, [0.017, 0.035]), showed reduced clustering (b = -0.044, [-0.062, -0.026]), a greater distance to the core (b = -0.031, [-0.043, -0.019]), as well as decreased efficiency (b = -0.004, [-0.005, -0.002]) and decreased strength (b = -0.057, [-0.079, -0.034]).

When visual information was read out, visual nodes had shorter paths to other nodes (b = -0.011, [-0.021, -0.002]) and were closer to the core (b = 0.018, [0.005, 0.030]). A summary of network analysis results is provided in Table 6.

Discussion

This study investigated how attending to auditory and visual information systematically changes graph theoretical measures of integration and functional connectivity between three

Table 6. Summary of results from network analysis.

	Auditory read-out			Visual read-out		
Connection strength	A–T	↑		V–T	↑	
	A–A	↑		A–A	↓	
	V–V	↓				
	V–A	↓				
Graph measures	Auditory nodes		Visual nodes		Auditory nodes		Visual nodes	
	PL	↓	PL	↑			PL	↓
	CL	↑	CL	↓				
	CCL	↑	CCL	↓			CCL	↑
	E	↑	E	↓				
	S	↑	S	↓				

Note. V = Visual module, A = Auditory module, T = task module (core); PL = characteristic path length, CL = clustering coefficient, CCL = core closeness, E = nodal efficiency, S = strength.

network modules: auditory, visual, and joint task core. Supporting our hypotheses, connection strength was increased between the task and the visual module when participants attended to colour, and between the task and the auditory module when they attended to pitch. Moreover, several nodal graph measures showed consistent changes to attentional modulation in form of stronger integration of sensory regions in response to attention. Together, these findings corroborate dynamical adjustments of both modality-specific and modality-independent functional brain networks in response to task demands and their representation in graph theoretical measures.

In a first step, we analyzed functional segregation, i.e., the specialization of a brain region for a specific function, to determine our network nodes. By computing BOLD contrasts, we established three sets of areas specific for visual read-out, for auditory read-out, and for the common task shared by both. Attention to either visual or auditory information provided by the audiovisual stimulus sequence led to enhanced activity in relevant sensory brain regions. The read-out of colour information led to activations in V2, V4, and inferior-temporal cortex which are all involved in colour processing [38–39]. Accompanying activity in the dorsal visual stream presumably resulted from the spatial arrangement of the colour-changing circles [40–41], but was omitted for node definition. In case of auditory read-out, we found bilateral activity in Heschl's gyrus (BA 41 and 42) reflecting pitch processing [42–43], and in posterior STG (BA 22) reflecting complex auditory processing, as required for chords and melodies [42, 44–45]. Right hemisphere activations were slightly more pronounced, as often found for music [42, 44–46]. No matter whether participants attended to pitch, colour, or both, the common task was translating pitch and colour information into the spatial domain to prepare for the upcoming visual search. This task elicited bilateral activity in the frontal eye fields/dorsal premotor cortex, superior parietal lobule, and intraparietal sulcus–brain regions known as the dorsal attention network (DAN; [47–50]). The DAN is involved in spatial and non-spatial allocation of attention [51–53] and arbitrary sensorimotor mapping [54–56], both crucial functions for the present task. Notably, DAN activity is not restricted to the visual domain but also found for touch [57–58] and audition [59–61], illustrating the network's multimodality [62–63]. As for all fronto-parietal networks residing in the association cortex, the DAN is highly and reciprocally interconnected to lower-level primary and secondary sensory cortices [64–66], making it the ideal core among our network modules.

In a second step, we analyzed functional integration, i.e., the coordinative coupling of functionally distinct brain regions. Peak voxels of the calculated BOLD contrasts constituted the centers of our network nodes, and every node was assigned to either the visual, auditory, or task network (core). Note that the definition of our core was not based on graph theoretical measures but theoretical assumptions. We were particularly interested in the interaction between core and sensory modules and the functional integration of individual nodes. Functional connectivity between nodes was measured in terms of (Z-transformed) Pearson correlations between two nodes' BOLD time series, and weighted graph measures were based on all positive correlations. The graph theoretical analysis revealed that several nodal graph measures were sensitive to attentional modulation. During auditory read-out, auditory nodes were characterised by shorter characteristic paths, increased node strength, increased nodal efficiency as well as increased clustering. These measures can be interpreted as reflecting enhanced network communication and, therefore, stronger integration [24]. Interestingly, the opposite pattern was observed for visual nodes in the same periods, which means that they were less integrated when attention was directed to auditory information. In contrast, when visual information was read out, visual nodes exhibited shorter paths, which again demonstrated enhanced integration during attention. In accordance with our hypotheses, attention to either visual or auditory information led to enhanced integration of corresponding sensory nodes. Visual nodes

even showed reduced integration when attention was directed to audition. Although not part of our original hypotheses, the finding of reduced integration of visual nodes during auditory task-relevance replicates the results from an earlier study [20] and demonstrates the network's ability to flexibly adapt to current task demands. More specifically, both studies reported reduced clustering as well as core closeness for task-irrelevant areas. Conceptually, the clustering coefficient reflects interconnectivity, meaning that a highly clustered network consists of nodes whose neighbours are themselves neighbours. Reduced clustering of visual nodes during auditory read-out—importantly, along with *enhanced* clustering of auditory nodes—thus reflects an exceptionally effective adaptation of network connectivity. Fittingly, reduced core closeness of visual nodes during auditory read-out (again, along with *enhanced* core closeness of auditory nodes) shows that not only within-module connections but also core-periphery interactions were flexibly and efficiently reorganised to fit current task demands. Our results thus further extend previous findings in that enhanced integration measures are not specific to the visual system but also apply to auditory circuits, indicating a modality-independent adaptive process.

To further assess the interactions between sensory modules and task core, we considered effects of visual and auditory attention on within-module and between-modules connection strength by fitting a GLMM. The analysis of between-modules connections revealed a dynamic, task-dependent coupling of our task core and sensory modules. As hypothesised, modality-specific regions were more strongly connected to the task core when the corresponding modality was attended to. Previous studies have shown this separately for the visual [67–71] and the auditory domain [72], whereas our study is the first to demonstrate this effect for both modalities within one experiment and based on combined audiovisual stimuli. Our results suggest that during attention, core-periphery communication is dynamically adjusted to fulfill task demands. While core-periphery communication was equally modulated by attention for both visual and auditory modules, we found reduced connection strength within the module processing the unattended modality as well as increased connection strength within the auditory module in case of auditory read-out. Notably, the latter effect was absent for the visual module during visual read-out. These results are in contrast to studies reporting reduced connection strength within the visual module in a visual task when compared to rest [69] or passive viewing [71]. Thus, further work is needed to clarify differences between visual and auditory within-module modulation.

Conclusion

Using a graph theoretical analysis approach to task-based fMRI, core-periphery interaction and integration for vision and audition can be demonstrated within one experiment and based on the same stimuli. In response to visual and auditory selective attention, increased functional connectivity between task-relevant sensory regions and the dorsal attention network, and nodal graph measures signify enhanced integration of sensory nodes in response to attention. These findings illustrate the brain's ability to dynamically adjust network communication to fulfill task-demands. Given that the use of graph theoretical measures in task-based fMRI research is still in its infancy, this study adds to the recently burgeoning evidence that graph measures are valuable for capturing dynamic cognitive processes.

Supporting information

S1 Table. Description, formula, value range, response distribution, and link function of analyzed graph measures.
(DOCX)

S2 Table. Mean, standard deviation, and range of all conditions for the assessed graph measures and connection strength.
(DOCX)

Acknowledgments

Author Contributions

Conceptualization: Laura Quante, Daniel S. Kluger, Matthias Ekman, Ricarda I. Schubotz.

Data curation: Laura Quante, Daniel S. Kluger.

Formal analysis: Laura Quante, Paul C. Bürkner, Matthias Ekman.

Investigation: Laura Quante.

Methodology: Laura Quante, Daniel S. Kluger, Matthias Ekman, Ricarda I. Schubotz.

Project administration: Ricarda I. Schubotz.

Supervision: Ricarda I. Schubotz.

Visualization: Laura Quante, Daniel S. Kluger.

Writing – original draft: Laura Quante, Daniel S. Kluger.

Writing – review & editing: Laura Quante, Daniel S. Kluger, Paul C. Bürkner, Matthias Ekman, Ricarda I. Schubotz.

References

1. Tononi G, Sporns O, Edelman GM. A measure for brain complexity: relating functional segregation and integration in the nervous system. Proc Natl Acad Sci USA. 1994; 91: 5033–5037. PMID: 8197179

2. Friston K. Beyond phrenology: what can neuroimaging tell us about distributed circuitry? Annu Rev Neurosci. 2002; 25: 221–250. https://doi.org/10.1146/annurev.neuro.25.112701.142846 PMID: 12052909

3. Sporns O. Network attributes for segregation and integration in the human brain. Curr Opin Neurobiol. 2013; 23: 162–171. https://doi.org/10.1016/j.conb.2012.11.015 PMID: 23294553

4. Beckmann CF, DeLuca M, Devlin JT, Smith SM. Investigations into resting-state connectivity using independent component analysis. Philos Trans R Soc Lond B Biol Sci. 2005; 360: 1001–1013. https://doi.org/10.1098/rstb.2005.1634 PMID: 16087444

5. Damoiseaux JS, Rombouts SARB, Barkhof F, Scheltens P, Stam CJ, Smith SM, et al. Consistent resting-state networks across healthy subjects. Proc Natl Acad Sci USA. 2006; 103: 13848–13853. https://doi.org/10.1073/pnas.0601417103 PMID: 16945915

6. De Luca M, Beckmann CF, De Stefano N, Matthews PM, Smith SM. fMRI resting state networks define distinct modes of long-distance interactions in the human brain. Neuroimage. 2006; 29: 1359–1367. https://doi.org/10.1016/j.neuroimage.2005.08.035 PMID: 16260155

7. Smith SM, Fox PT, Miller KL, Glahn DC, Fox PM, Mackay CE, et al. Correspondence of the brain's functional architecture during activation and rest. Proc Natl Acad Sci USA. 2009; 106: 13040–13045. https://doi.org/10.1073/pnas.0905267106 PMID: 19620724

8. Power JD, Cohen AL, Nelson SM, Wig GS, Barnes KA, Church JA, et al. Functional network organization of the human brain. Neuron. 2011; 72: 665–678. https://doi.org/10.1016/j.neuron.2011.09.006 PMID: 22099467

9. Hagmann P, Cammoun L, Gigandet X, Meuli R, Honey CJ, Wedeen VJ, et al. Mapping the structural core of human cerebral cortex. PLoS Biology. 2008; 6: e159. https://doi.org/10.1371/journal.pbio.0060159 PMID: 18597554

10. van den Heuvel MP, Sporns O. Rich-club organization of the human connectome. J Neurosci. 2011; 31: 15775–15786. https://doi.org/10.1523/JNEUROSCI.3539-11.2011 PMID: 22049421

11. van den Heuvel MP, Kahn RS, Goñi J, Sporns O. High-cost, high-capacity backbone for global brain communication. Proc Natl Acad Sci USA. 2012; 109: 11372–11377. https://doi.org/10.1073/pnas.1203593109 PMID: 22711833

12. van den Heuvel MP, Sporns O. An anatomical substrate for integration among functional networks in human cortex. J Neurosci. 2013, 33: 14489–14500. https://doi.org/10.1523/JNEUROSCI.2128-13.2013 PMID: 24005300

13. Shanahan M. The brain's connective core and its role in animal cognition. Philos Trans R Soc Lond B Biol Sci. 2012; 367: 2704–2714. https://doi.org/10.1098/rstb.2012.0128 PMID: 22927569

14. Tognoli E, Kelso JS. The metastable brain. Neuron. 2014; 81: 35–48. https://doi.org/10.1016/j.neuron.2013.12.022 PMID: 24411730

15. Kinnison J, Padmala S, Choi JM, Pessoa L. Network analysis reveals increased integration during emotional and motivational processing. J Neurosci. 2012; 32: 8361–8372. https://doi.org/10.1523/JNEUROSCI.0821-12.2012 PMID: 22699916

16. Andric M, Hasson U. Global features of functional brain networks change with contextual disorder. Neuroimage. 2015; 117: 103–113. https://doi.org/10.1016/j.neuroimage.2015.05.025 PMID: 25988223

17. Vatansever D, Menon DK, Manktelow AE, Sahakian BJ, Stamatakis EA. Default mode dynamics for global functional integration. J Neurosci. 2015; 35: 15254–15262. https://doi.org/10.1523/JNEUROSCI.2135-15.2015 PMID: 26586814

18. Cohen JR, D'Esposito M. The segregation and integration of distinct brain networks and their relationship to cognition. J Neurosci. 2016; 36: 12083–12094. https://doi.org/10.1523/JNEUROSCI.2965-15.2016 PMID: 27903719

19. Cole MW, Reynolds JR, Power JD, Repovs G, Anticevic A, Braver TS. Multi-task connectivity reveals flexible hubs for adaptive task control. Nat Neurosci. 2013; 16: 1348. https://doi.org/10.1038/nn.3470 PMID: 23892552

20. Ekman M, Derrfuss J, Tittgemeyer M, Fiebach CJ. Predicting errors from reconfiguration patterns in human brain networks. Proc Natl Acad Sci USA. 2012; 109: 16714–16719. https://doi.org/10.1073/pnas.1207523109 PMID: 23012417

21. Whitfield-Gabrieli S, Nieto-Castanon A. Conn: a functional connectivity toolbox for correlated and anticorrelated brain networks. Brain Connect. 2012; 2: 125–141. https://doi.org/10.1089/brain.2012.0073 PMID: 22642651

22. Behzadi Y, Restom K, Liau J, Liu TT. A component based noise correction method (CompCor) for BOLD and perfusion based fMRI. Neuroimage. 2007; 37: 90–101. https://doi.org/10.1016/j.neuroimage.2007.04.042 PMID: 17560126

23. Ekman M, Fiebach CJ, Melzer C, Tittgemeyer M, Derfuss J. Different roles of direct and indirect frontoparietal pathways for individual working memory capacity. J Neurosci. 2016; 36: 2894–2903. https://doi.org/10.1523/JNEUROSCI.1376-14.2016 PMID: 26961945

24. Rubinov M, Sporns O. Complex network measures of brain connectivity: uses and interpretations. Neuroimage. 2010; 52: 1059–1069. https://doi.org/10.1016/j.neuroimage.2009.10.003 PMID: 19819337

25. Gelman A, Hill J. Data analysis using regression and multilevel/hierarchical models. Cambridge: Cambridge UP; 2006.

26. Tuerlinckx F, Rijmen F, Verbeke G, Boeck P. Statistical inference in generalized linear mixed models: A review. Br J Math Stat Psychol. 2006; 59: 225–255. https://doi.org/10.1348/000711005X79857 PMID: 17067411

27. Bürkner PC. brms: An R package for Bayesian multilevel models using Stan. J Stat Softw. 2016; 80: 1–28.

28. Bürkner PC. Advanced Bayesian Multilevel Modeling with the R Package brms. The R Journal. 2018; Forthcoming.

29. Carpenter B, Gelman A, Hoffman MD, Lee D, Goodrich B, Betancour M, Brubaker MA, et al. Stan: A probabilistic programming language. J Stat Softw. 2017; 76: 1–43.

30. Kruschke JK, Vanpaemel W. Bayesian estimation in hierarchical models. In: Busemeyer J, Townsend J, Wang ZJ, Eidels A, editors. The Oxford Handbook of Computational and Mathematical Psychology. Oxford: Oxford UP; 2015. pp. 279–299.

31. Kruschke JK, Liddell TM. The Bayesian New Statistics: Hypothesis testing, estimation, meta-analysis, and power analysis from a Bayesian perspective. Psychon Bull Rev. 2018; 25: 178–206. https://doi.org/10.3758/s13423-016-1221-4 PMID: 28176294

32. Hoffman MD, Gelman A. The No-U-turn sampler: adaptively setting path lengths in Hamiltonian Monte Carlo. J Mach Learn Res. 2014; 15: 1593–1623.

33. De Vico Fallani F, Richiardi J, Chavez M, Achard S. Graph analysis of functional brain networks: practical issues in translational neuroscience. Philos Trans R Soc Lond B Biol Sci. 2014; 369: 1–17.

34. Gelman A, Rubin DB. Inference from iterative simulation using multiple sequences. Stat Sci. 1992; 457–472.

35. Xia M, Wang J, He Y. BrainNet Viewer: a network visualization tool for human brain connectomics. PLOS One. 2013; 8: e68910. https://doi.org/10.1371/journal.pone.0068910 PMID: 23861951

36. Bastian M, Heymann S, Jacomy M. Gephi: an open source software for exploring and manipulating networks. Proceedings of the Third International ICWSM Conference. 2009; 361–362.

37. Jacomy M, Venturini T, Heymann S, Bastian M. ForceAtlas2, a continuous graph layout algorithm for handy network visualization designed for the Gephi software. PLOS One. 2014; 9: e98679. https://doi.org/10.1371/journal.pone.0098679 PMID: 24914678

38. Gegenfurtner KR. Cortical mechanisms of colour vision. Nat Rev Neurosci. 2003; 4: 563–572. https://doi.org/10.1038/nrn1138 PMID: 12838331

39. Shapley R, Hawken MJ. Color in the cortex: single-and double-opponent cells. Vision Res. 2011; 51: 701–717. https://doi.org/10.1016/j.visres.2011.02.012 PMID: 21333672

40. Rizzolatti G, Matelli M.Two different streams form the dorsal visual system: anatomy and functions. Exp Brain Res. 2003; 153: 146–157. https://doi.org/10.1007/s00221-003-1588-0 PMID: 14610633

41. Perry CJ, Fallah M. Feature integration and object representations along the dorsal stream visual hierarchy. Front Comput Neurosci. 2014; 8: 1–17. https://doi.org/10.3389/fncom.2014.00001 PMID: 24550816

42. Koelsch S. Toward a neural basis of music perception–a review and updated model. Front Psychol. 2011; 2: 1–20. https://doi.org/10.3389/fpsyg.2011.00001 PMID: 21713130

43. Alho K, Rinne T, Herron TJ, Woods DL. Stimulus-dependent activations and attention-related modulations in the auditory cortex: a meta-analysis of fMRI studies. Hear Res. 2014; 307: 29–41. https://doi.org/10.1016/j.heares.2013.08.001 PMID: 23938208

44. Griffiths TD, Warren JD. The planum temporale as a computational hub. Trends Neurosci. 2002; 25: 348–353. PMID: 12079762

45. Griffiths TD. Functional imaging of pitch analysis. Ann N Y Acad Sci. 2003; 999: 40–49. PMID: 14681116

46. Zatorre RJ, Belin P, Penhune VB. Structure and function of auditory cortex: music and speech. Trends Cogn Sci. 2002; 6: 37–46. PMID: 11849614

47. Corbetta M, Shulman GL. Control of goal-directed and stimulus-driven attention in the brain. Nat Rev Neurosci. 2002; 3: 201–215. https://doi.org/10.1038/nrn755 PMID: 11994752

48. Fox MD, Snyder AZ, Vincent JL, Corbetta M, Van Essen DC, Raichle ME. The human brain is intrinsically organized into dynamic, anticorrelated functional networks. Proc Natl Acad Sci USA. 2005; 102: 9673–9678. https://doi.org/10.1073/pnas.0504136102 PMID: 15976020

49. Ptak R. The frontoparietal attention network of the human brain: action, saliency, and a priority map of the environment. Neuroscientist. 2012; 18: 502–515. https://doi.org/10.1177/1073858411409051 PMID: 21636849

50. Vossel S, Geng JJ, Fink GR. Dorsal and ventral attention systems: distinct neural circuits but collaborative roles. Neuroscientist. 2014; 20: 150–159. https://doi.org/10.1177/1073858413494269 PMID: 23835449

51. Egner T, Monti JM, Trittschuh EH, Wieneke CA, Hirsch J, Mesulam MM. Neural integration of top-down spatial and feature-based information in visual search. J Neurosci. 2008; 28: 6141–6151. https://doi.org/10.1523/JNEUROSCI.1262-08.2008 PMID: 18550756

52. Liu T, Hospadaruk L, Zhu DC, Gardner JL. Feature-specific attentional priority signals in human cortex. J Neurosci. 2011; 31: 4484–4495. https://doi.org/10.1523/JNEUROSCI.5745-10.2011 PMID: 21430149

53. Jerde TA, Merriam EP, Riggall AC, Hedges JH, Curtis CE. Prioritized maps of space in human frontoparietal cortex. J Neurosci. 2012; 32: 17382–17390. https://doi.org/10.1523/JNEUROSCI.3810-12.2012 PMID: 23197729

54. Wise SP, Di Pellegrino G, Boussaoud D. The premotor cortex and nonstandard sensorimotor mapping. Can J Physiol Pharmacol. 1996; 74: 469–482. PMID: 8828893

55. Grefkes C, Fink GR. The functional organization of the intraparietal sulcus in humans and monkeys. J Anat. 2005; 207: 3–17. https://doi.org/10.1111/j.1469-7580.2005.00426.x PMID: 16011542

56. Brovelli A, Badier JM, Bonini F, Bartolomei F, Coulon O, Auzias G. Dynamic reconfiguration of visuomotor-related functional connectivity networks. J Neurosci. 2017; 37: 839–853. https://doi.org/10.1523/JNEUROSCI.1672-16.2016 PMID: 28123020

57. Macaluso E, Driver J. Spatial attention and crossmodal interactions between vision and touch. Neuropsychologia. 2001; 39: 1304–1316. PMID: 11566313

58. Macaluso E, Frith CD, Driver J. Supramodal effects of covert spatial orienting triggered by visual or tactile events. J Cogn Neurosci. 2002; 14: 389–401. https://doi.org/10.1162/089892902317361912 PMID: 11970799

59. Shomstein S, Yantis S. Control of attention shifts between vision and audition in human cortex. J Neurosci. 2004; 24: 10702–10706. https://doi.org/10.1523/JNEUROSCI.2939-04.2004 PMID: 15564587

60. Smith DV, Davis B, Niu K, Healy EW, Bonilha L, Fridriksson J, et al. Spatial attention evokes similar activation patterns for visual and auditory stimuli. J Cogn Neurosci. 2010; 22: 347–361. https://doi.org/10.1162/jocn.2009.21241 PMID: 19400684

61. Green JJ, Doesburg SM, Ward LM, McDonald JJ. Electrical neuroimaging of voluntary audiospatial attention: evidence for a supramodal attention control network. J Neurosci. 2011; 31: 3560–3564. https://doi.org/10.1523/JNEUROSCI.5758-10.2011 PMID: 21389212

62. Macaluso E & Driver J. Multisensory spatial interactions: a window onto functional integration in the human brain. Trends Neurosci. 2005; 28: 264–271. https://doi.org/10.1016/j.tins.2005.03.008 PMID: 15866201

63. Macaluso E. Orienting of spatial attention and the interplay between the senses. Cortex. 2010; 46: 282–297. https://doi.org/10.1016/j.cortex.2009.05.010 PMID: 19540475

64. Bressler SL, Tang W, Sylvester CM, Shulman GL, Corbetta M. Top-down control of human visual cortex by frontal and parietal cortex in anticipatory visual spatial attention. J Neurosci. 2008; 28: 10056–10061. https://doi.org/10.1523/JNEUROSCI.1776-08.2008 PMID: 18829963

65. Vossel S, Weidner R, Driver J, Friston KJ, Fink GR. Deconstructing the architecture of dorsal and ventral attention systems with dynamic causal modeling. J Neurosci. 2012; 32: 10637–10648. https://doi.org/10.1523/JNEUROSCI.0414-12.2012 PMID: 22855813

66. Yeo BT, Krienen FM, Chee MW, Buckner RL. Estimates of segregation and overlap of functional connectivity networks in the human cerebral cortex. Neuroimage. 2014; 88: 212–227. https://doi.org/10.1016/j.neuroimage.2013.10.046 PMID: 24185018

67. Chadick JZ, Gazzaley A. Differential coupling of visual cortex with default or frontal-parietal network based on goals. Nat Neurosci. 2011; 14: 830–832. https://doi.org/10.1038/nn.2823 PMID: 21623362

68. Alnæs D, Kaufmann T, Richard G, Duff EP, Sneve MH, Endestad T, et al. Attentional load modulates large-scale functional brain connectivity beyond the core attention networks. Neuroimage. 2015; 109: 260–272. https://doi.org/10.1016/j.neuroimage.2015.01.026 PMID: 25595500

69. Spadone S, Della Penna S, Sestieri C, Betti V, Tosoni A, Perrucci MG, et al. Dynamic reorganization of human resting-state networks during visuospatial attention. Proc Natl Acad Sci USA. 2015; 112: 8112–8117. https://doi.org/10.1073/pnas.1415439112 PMID: 26080395

70. Wen X, Zhang D, Liang B, Zhang R, Wang Z, Wang J, et al. Reconfiguration of the brain functional network associated with visual task demands. PLOS One. 2015; 10: e0132518. https://doi.org/10.1371/journal.pone.0132518 PMID: 26146993

71. Kwon S, Watanabe M, Fischer E, Bartels A. Attention reorganizes connectivity across networks in a frequency specific manner. Neuroimage. 2017; 144: 217–226. https://doi.org/10.1016/j.neuroimage.2016.10.014 PMID: 27732887

72. Sadaghiani S, Poline JB, Kleinschmidt A, D'Esposito M. Ongoing dynamics in large-scale functional connectivity predict perception. Proc Natl Acad Sci USA. 2015; 112: 8463–8468. https://doi.org/10.1073/pnas.1420687112 PMID: 26106164